Journal Name

ARTICLE

Ultrafast Electron Transfer in All-Carbon-Based SWCNT-C_{60} Donor-Acceptor Nanoensembles Connected by Poly(phenylene-ethynylene) Spacers

Received 00th January 20xx,
Accepted 00th January 20xx

DOI: 10.1039/x0xx00000x

www.rsc.org/

Myriam Barrejón,[a] Habtom B. Gobeze,[b] María J. Gómez-Escalonilla,[a] José Luis G. Fierro,[c] Minfang Zhang,[d] Masako Yudasaka,[d] Sumio Iijima,[d,e] Francis D'Souza[b]* and Fernando Langa[a]*

Building all-carbon based functional materials for light energy harvesting applications could be a solution to tackle and reduce environmental carbon output. However, development of such all-carbon based donor-acceptor hybrids and demonstration of photoinduced charge separation in such nanohybrids is a challenge since in these hybrids part of the carbon material should act as an electron donating or accepting photosensitizer while the second part should fulfil the role of an electron acceptor or donor. In the present work, we have successfully addressed this issue by synthesizing covalently linked all-carbon-based donor-acceptor nanoensembles using single-walled carbon nanotubes (SWCNTs) as the donor and C_{60} as an acceptor. The donor-acceptor entities in the nanoensembles were connected by phenylene-ethynylene spacer units to achieve better electronic communication and to vary the distance between the components. These novel SWCNT-C_{60} nanoensembles have been characterized by a number of techniques, including TGA, FT-IR, Raman, AFM, absorbance and electrochemical methods. The moderate number of fullerene addends present on the side-walls of the nanotubes largely preserved the electronic structure of the nanotubes. The thermodynamic feasibility of charge separation in these nanoensembles was established using spectral and electrochemical data. Finally, occurrence of ultrafast electron transfer from the excited nanotubes in these donor-acceptor nanohybrids has been established from femtosecond transient absorption studies, signifying their utility in building light energy harvesting devices.

Dedicated to Prof. Nazario Martin on the occasion of his 60th bitrhday.

1. Introduction

Single-walled carbon nanotubes (SWCNTs) and fullerene (C_{60}) in nanoensemble materials have attracted increased attention in recent years for high efficiency photovoltaic devices.[1-21] These materials are particularly important considering that both donor and acceptor entities are all-carbon materials, thus providing a natural way to combat environmental carbon problems by employing them as energy harvesting functional materials.[22-23] In one such example, a thin film of chirality-sorted semiconducting SWCNTs combined with the electron-acceptor fullerene have shown internal quantum efficiencies greater than 85% with moderate power conversion efficiencies [24-26] in their bilayer (~1%)[27] and bulk heterojunction (~1.7%)[28] configurations. In order to improve the efficiencies of these devices it is necessary to have a greater understanding of the ways in which photoinduced processes can be modulated.[29-31] This goal could be achieved by covalent or noncovalent functionalization of SWCNT-C_{60} hybrid materials. A literature survey on SWCNT-C_{60} shows that there are only two examples of this class of nanoensemble formed in a self-assembled supramolecular fashion.[32,33] While the self-assembly approach preserves the π-electronic structure of the nanotubes without converting sp^2 carbons to sp^3 carbons, the dynamic nature of the self-assembled systems often makes it difficult to derive meaningful structure-reactivity relationships.

In an effort to overcome this critical issue, in the present study the SWCNT and C_{60} are covalently linked using phenylene ethynylene spacer units (see Fig. 1 for structures), which have good electronic communication. Additionally, the number of fullerene addends on the nanotube surface is limited to a modest number in order to avoid compromising the π-electronic structure of the nanotubes. Further, solubility of the nanoensembles is improved by functionalizing the fullerene entity with two long $–OC_{12}H_{25}$ chains. The synthesis,

[a] Universidad de Castilla-La Mancha, Instituto de Nanociencia, Nanotecnología y Materiales Moleculares (INAMOL), 45071-Toledo, Spain. E-mail: Fernando.Langa@uclm.es
[b] Department of Chemistry, University of North Texas, 1155 Union Circle, #305070, 76203-5017, Denton, TX, USA. E-mail: Francis.DSouza@UNT.edu
[c] Instituto de Catálisis y Petroleoquímica, CSIC, Cantoblanco, 28049, Madrid, Spain.
[d] Nanotube Research Center, National Institute of Advanced Industrial and Technology, Higashi, Tsukuba, Ibaraki 305-8565, Japan. E-mail: m-yudasaka@aist.go.jp
[e] Department of Physics, Meijo University, Shiogamaguchi, Tenpaku-ku, Nagoya 468-8502, Japan.

† Electronic Supplementary Information (ESI) available: Synthesis, TGA, FTIR, AFM and XPS data, UV-vis and transient absorption spectra (Fig. S1–S15 and Tables S1 and S2). See DOI: 10.1039/x0xx00000x.

characterization and photochemical processes for these nanoensembles were systematically investigated and the results are reported here.

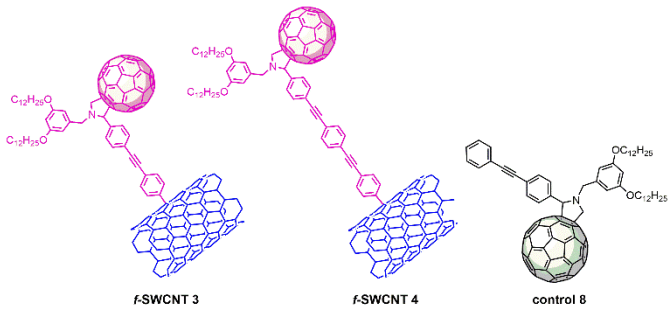

Fig. 1 Structures of SWCNT-C_{60} **3-4** nanoensembles connected with phenylene-ethynylene spacer units investigated in the present study and control compound **8**.

2. Experimental

2.1. Materials and methods

HIPCo SWCNTs were purchased from NanoIntegris (purified grade) with an individual diameter between 0.8 and 1.2 nm and length between 100 and 1000 nm. Pyrrolidinofullerene derivative **7** was prepared according the literature procedure.[34] Chemicals and solvents were purchased from Sigma-Aldrich. All air-sensitive reactions were carried out under argon atmosphere. Sample sonication was carried out by using an Elmasonic P 300 H sonicator bath (37 kHz). Microwaves reactions were performed in a CEM Discover reactor, equipped with fiber optic temperature detector and pressure control. ^{1}H NMR spectra were obtained on Bruker TopSpin Avance-400 (400 MHz) spectrometer. Chemical shifts are reported in parts per million (ppm) relative to the solvent residual peak ($CDCl_3$, 7.27 ppm). ^{13}C NMR chemical shifts are reported relative to the solvent residual peak ($CDCl_3$, 77.00 ppm). Steady-state absorption spectra in the visible region were measured on a Shimadzu UV 3600 spectrometer. IR spectra were obtained on a Fourier Transform IR spectrometer (Avatar 370) in KBr pellets. Raman spectra were performed on Renishaw inVia Raman microscope instrument at room temperature with a 785 nm exciting laser. Thermogravimetric analyses were performed under nitrogen atmosphere using a Mettler-Toledo model TGA/SDTA851e with a heating rate of 10 ºC/min. AFM images were acquired in tapping mode using a Multimode V8.10 (Veeco Instruments Inc., Santa Barbara, USA) with a NanoScope V controller (Digital Instruments, Santa Barbara, USA). The cantilevers (RTESP from Bruker Probes) with silicon cantilevers worked with a resonance frequency of 300 kHz and a nominal force constant of 40 Nm^{-1}. The functionalized samples (1 mg mL^{-1}) were prepared by sonication (frequency: 37 kHz; power 380 W) in milli-Q water and SBDS for 90 min. Samples were then drop-casted on SiO_2 surfaces. TEM observations were carried out using TOPCON002B (Topcon Corporation) at an acceleration voltage of 120 kV. X-ray photoelectron spectra were recorded with a VG 200R spectrometer equipped with a hemispherical electron analyzer and a Mg Kα (hν = 1253.6 eV) X-ray source. The X-ray source operated at 12 keV and 100 mA. Survey and high-resolution spectra were collected at 65° to the detector with pass energy resolutions of 200 and 50 eV, respectively. The linearity of the binding energy scale was calibrated against the Au $4f_{7/2}$ (84.0 eV) and the Cu $2p_{3/2}$ (932.6 eV) photoemission lines by standard procedures. Each sample was first placed in an aluminium holder mounted on a sample-rod placed in the pretreatment chamber of the spectrometer and then it was degassed at ambient temperature for 1 h before being transferred to the analysis chamber. Residual pressure within the ion-pumped analysis chamber was kept below $7x10^{-9}$ mbar during data acquisition. Binding energies were calculated with respect to the C-(C,H) component of the C1s peak fixed at 284.8 eV. The high-resolution spectra for the regions of interest were curve fitted using XPS Peak software. After subtraction of a Shirley background, the peaks were fitted using a nonlinear, least squares routine with mixed Gauss–Lorentz (90/10) functions. A minimum set of Gauss–Lorentz functions was chosen in order to obtain a reasonable fit. Osteryoung Square Wave Voltammetry (OSWV) was performed at room temperature in argon-purged solutions in *o*-DCB/acetonitrile 4:1 solution. Tetrabutylammonium hexafluorophosphate ($TBAPF_6$) (0.1 M as supporting electrolyte) was purchased from Sigma- Aldrich and used without purification. Experiments were done in a cell equipped with glassy carbon working electrode and a platinum wire counter electrode. An $Ag/AgNO_3$ electrode was used as reference and checked against the ferrocene/ferrocenium couple (Fc/Fc^+) before and after each experiment.

Femtosecond transient absorption spectroscopy experiments were performed using an Ultrafast Femtosecond Laser Source (Libra) by Coherent incorporating diode-pumped, mode locked Ti:Sapphire laser (Vitesse) and diode-pumped intra cavity doubled Nd:YLF laser (Evolution) to generate a compressed laser output of 1.45 W. For optical detection, a Helios transient absorption spectrometer coupled with a femtosecond harmonics generator both provided by Ultrafast Systems was used. The source for the pump and probe pulses were derived from the fundamental output of Libra (Compressed output 1.45 W, pulse width 100 fs) at a repetition rate of 1 kHz. About 95% of the fundamental output of the laser was introduced into harmonic generator which produces second and third harmonics of 400 and 267 nm besides the fundamental 800 nm for excitation, while the rest of the output was used for generation of white light continuum. In the present study, the fundamental 800 nm, and second harmonic 400 nm excitation pump was used in all the experiments. Kinetic traces at appropriate wavelengths were assembled from the time-resolved spectral data. Data analysis was performed using Surface Xplorer software supplied by Helios manufacturer. All measurements were conducted in Ar degassed solutions at 298 K.

2.2. Synthesis

Preparation of *f*-SWCNT 1 and *f*-SWCNT 2

Pristine HIPCo SWCNTs (30 mg) were dispersed in *N*-methylpyrrolidinone (NMP) (250 mL) by ultrasonication for 10 min. Nitrogen was bubbled through the suspension for 2 min

and the corresponding aniline (10 mmol) and isoamyl nitrite (10 mmol) were added. The mixture was allowed to react for 24 h at 70 ºC. The mixture was cooled to room temperature, the suspension was filtered through a PTFE (2 µm) membrane and washed repeatedly with *N,N*-dimethylformamide (DMF), methanol and diethyl ether, until the filtrate solution remained colourless. The material was dried overnight in a vacuum oven at 55 °C to afford functionalized materials **1** and **2.**

Preparation of *f*-SWCNT 3 and *f*-SWCNT 4

To a suspension of *f*-SWCNT **1** (or *f*-SWCNT **2**) (15 mg) in *o*-dichlorobenzene (40 mL) was added the corresponding fulleropyrrolidine **7**[34] (30 mg, 0.025 mmol), [Pd(Ph$_3$)$_4$] (10% mol) and a large excess of piperidine (3 mL). The mixture was heated using microwave irradiation (50 W) in a sealed tube for 60 min. The mixture was cooled to room temperature, the solid was centrifuged, the solvent was decanted off and the remaining solid was washed several times with methanol and dichloromethane (CH_2Cl_2) (sonicated, centrifuged and filtered) until the filtrate remained colourless, thus affording *functionalized* SWCNTs **3** and **4**.

3. Results and discussion

The methodology developed for the synthesis of SWCNT-C_{60} nanoensembles **3** and **4** is depicted in Scheme 1. The synthesis of the conjugated oligo(phenylene-ethynylene) (OPEs) precursors was carried out according to the Sonogashira coupling procedure described in the literature[35](see Scheme S1 in ESI†). In a parallel route, *pristine* SWCNTs were covalently functionalized by the widely applied methodology involving the addition of *in situ* generated aryl diazonium salts[36] by adding the corresponding 4-(2-trimethylsilyl)ethynylaniline derivative (see Scheme S2) in the presence of isoamyl nitrite in NMP to afford the appropriately functionalized nanotubes (*f*-SWCNTs **1** and **2**). Successive cleavage of the TMS groups with tetra-*n*-butylammonium fluoride (TBAF) afforded the corresponding deprotected nanotubes (see Scheme 1). Finally, pyrrolidinofullerene building block **7**[34] was grafted onto the corresponding deprotected nanotube by a copper-free Sonogashira C–C cross-coupling reaction.[37] This procedure was used to react compound **7** and the two deprotected nanotube derivatives in *o*-dichlorobenzene (*o*-DCB) under microwave irradiation[38] (50 W) at 150 ºC in a CEM discover microwave irradiator for 1 hour in the presence of piperidine and 10 mol% [Pd(Ph$_3$)$_4$] to give the coupled nanoconjugates *f*-SWCNT-**3** and **4**.

A control fulleropyrrolidine sample **8** (see ESI†, Scheme S3) was also prepared as a reference for electrochemical and photophysical measurements with nanohybrids **3** and **4.**

The successful preparation of nanoensembles **3** and **4** was confirmed by a wide range of analytical techniques, including thermogravimetric analysis (TGA), Fourier transform infrared spectroscopy (FTIR), atomic force microscopy (AFM), high-resolution transmission electron microscopy (HR-TEM), Raman spectroscopy, X-ray photoelectron spectroscopy (XPS) and steady-state and time-resolved spectroscopic techniques.

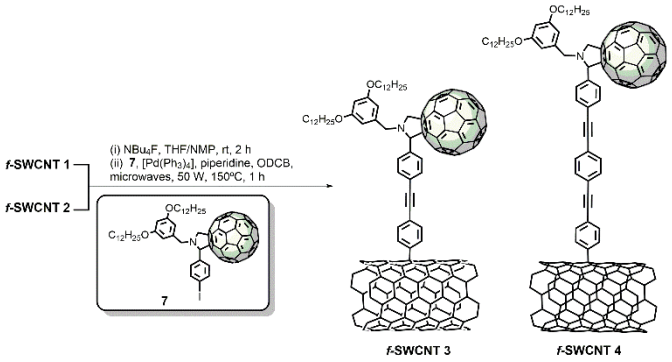

Scheme 1 Synthetic route for the preparation of nanoensembles **3** and **4**.

In order to estimate the degree of functionalization of the nanotubes, thermogravimetric analysis (TGA) was carried out under a nitrogen flow with a heating rate of 10 ºC/min up to 1000 ºC. The thermal behavior of the functionalized materials is represented in Figure S1† along with that of *pristine* SWCNT and the control fulleropyrrolidine **8**. The thermogram of *f*-SWCNT **1** shows a weight loss of 15% at 550 ºC (Figure S1, left). An additional weight loss of 19% was observed for *f*-SWCNT **3** and this is directly related to the decomposition of the fulleropyrrolidine derivative **8**. Considering the thermogram of the fulleropyrrolidine (39% weight loss at 550 ºC), the actual weight loss corresponding to the nanoconjugate **3** is 48% at this temperature, which is approximately one group for each 241 carbon atoms of the nanotube. In a similar way, a weight loss of 18% was observed at 550 ºC for *f*-SWCNT **2** (see Figure S1, right). Nanoensemble **4** shows an additional weight loss of 15.5%. The actual weight loss corresponding to *f*-SWCNT **4** is 38% at 550 ºC, which is approximately one group for each 310 carbon atoms of the nanotube.

The Raman spectra of nanohybrids **3** and **4** were compared to those of the precursors **1** and **2**, the control fulleropyrrolidine **8** and *pristine* SWCNT in an effort to evaluate the effect of the derivatization. As shown in Figs. 2 and S2†, the Raman spectrum (λ = 785 nm) of *pristine* SWCNT shows an intense tangential mode (G band) at 1593 cm^{-1} and a disorder-induced peak (D band) at 1290 cm^{-1}. After the first functionalization, the intensity of the I_D/I_G ratio for **1** and **2** increased [0.35 for **1** and 0.62 for **2**] when compared to that of *pristine* SWCNT (0.07) due to the incorporation of the aryl moieties onto the skeleton of the CNTs. A further increase was not observed on changing from *f*-SWCNT **1** to **3** and *f*-SWCNT **2** to **4**, since the Sonogashira coupling takes place on the triple bonds rather than directly on the nanotube surface. In addition, the signature of the Ag(2) mode of C_{60}, which in the control **8** appears at 1469 cm^{-1}, was observed at 1462 cm^{-1} and 1420 cm^{-1} for *f*-SWCNT **3** and **4**, respectively, and this confirms that the cross coupling had occurred.[39,4]

X-ray photoelectron spectroscopy (XPS) was used to investigate the synthesis of functionalized SWCNTs **3** and **4** by directly comparing the C 1s and N 1s core-level spectra of the precursors and the synthesized materials. The XP survey scan allows the unambiguous identification of the elements present on solid surfaces and, as a consequence, a low resolution, wide

energy scan was first recorded on all the samples. Moreover, high-resolution C 1s, O 1s and N 1s (together with Si 2p and I 3d, if present) spectra were recorded (see ESI†). The binding energies of core levels for *pristine* SWCNT, *f*-SWCNTs **1–4** and the pyrrolidinofullerene derivative **7** are included in Table S1†. The C 1s and O 1s spectra of the *pristine* SWCNT sample are displayed in Fig. S3†. According to the assignment by Boehm[41] and those in our previous studies,[42-44] the C 1s emission was satisfactorily curve-resolved with five components at 284.8, 286.3, 287.7, 289.2 and 291.3 eV: the most intense component at 284.8 eV is assigned to sp^2 C-atoms of the nanotube structure. This peak, together with the weak π–π* plasmon component at around 291.3 eV, is indicative of the C graphene structure of the SWCNT. The component at 286.3 eV is often assigned to C–OH, and the components at 287.7 and 289.2 eV to C=O and –COO– species, respectively (see Table S1 and Fig. S3†). Similarly, the O 1s line was curve-resolved with two components: the minor component at 531.6 eV corresponds to O=C surface groups whereas the major component at 533.2 eV is often associated with the O–C bond.[45]

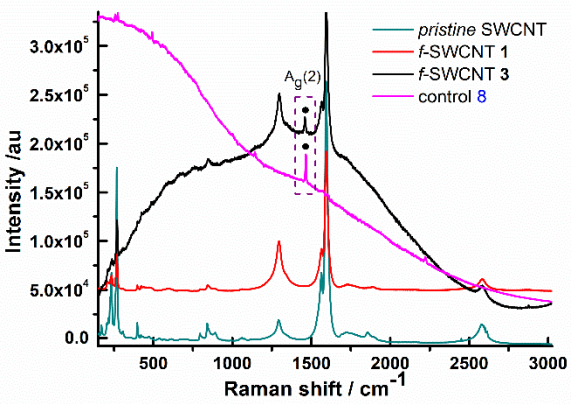

Fig. 2 Raman spectra of *pristine* SWCNT, the functionalized samples *f*-SWCNT **1** and **3** and the control sample **8**, λ_{exc} = 785 nm.

Binding energy values (BEs) of covalently functionalized SWCNT with the corresponding 4-(2-trimethylsilyl) ethynylaniline derivative (*f*-SWCNTs **1** and **2**) are also included in Table S1 (ESI†). For these samples, the Si 2p core-level of the TMS group appeared at a BE of 102.0–102.1 eV and this is consistent with reported values for such groups.[46] O 1s and C 1s profiles were similar to that of *pristine* SWCNT, with perhaps the only difference being that the π–π* loss feature at around 291.3 eV is almost non-existent after functionalization, which indicates the partial loss of the nanotube structure. From quantitative data (Table 1) it appears that the extent of Si incorporation is almost constant for *f*-SWCNT **1** (1.6% O atom) and *f*-SWCNT **2** (1.5% O atom).

The XP spectrum of fullerene derivative **7** is displayed in Table S1 and Table 1. The high-resolution N 1s core level spectrum of **7** (Fig. S4†) shows the component assigned to photoelectrons emitted from the N atom of tertiary amines, which is centered at 399.0 eV (the N 1s peak for the pyrrolidine ring[47]). Finally, it should be highlighted that fulleropyrrolidine **7** displayed the characteristic I 3d doublet (see Fig. S5 in ESI†), whose multiple splitting of $3d_{5/2}$ and $3d_{3/2}$ peaks of 11.5 eV and the BE of the most intense $I3d_{5/2}$ peak at 620.9 eV indicate the presence of some iodine-containing organic impurity retained from the synthesis.[48]

Table 1. Composition of SWCNT samples estimated from XPS signal intensities.

Sample	C (% at)	O (% at)	N (% at)	I (% at)	Si (% at)
Pristine SWCNT	95.7	4.3	-	-	-
7	90.6	4.7	2.4	2.3	-
f-SWCNT **1**	94.3	4.1	-	-	1.6
f-SWCNT **2**	94.7	3.8	-	-	1.5
f-SWCNT **3**	93.4	5.5	1.1	-	-
f-SWCNT **4**	93.5	5.4	1.1	-	-

Similarly, the XP spectra of the coupled nanoconjugates *f*-SWCNT **3** and **4** were recorded and the corresponding BE values for the C 1s, O 1s and N 1s core-levels are compiled in Table S1.† The binding energies of C 1s and O 1s peaks are similar to those of the respective *f*-SWCNT **1** and **2** precursors (Table S1†), but an N 1s peak at 399.0–399.1 eV was recorded (Fig. S4†) and this fits very well with the BE of the fulleropyrrolidine precursor **7**. The N contents for *f*-SWCNTs **3** and **4** (Table 1) are the same (1.1% atom) while the O content is slightly higher (5.4 and 5.5% atom) than that of the counterparts *f*-SWCNT **1** and **2**. This finding provides evidence for the anchorage of dodecyl alkyl chains in pyrrolidine derivative **7**. Indeed, detailed C 1s fitting[49] analysis indicated the presence of sp^3 C-atoms in derivative **7** as well as in hybrid materials **3** and **4** (Fig. S6†). This finding also supports the successful anchoring of fullerene derivative **7** onto the CNT-functionalized substrates.

The FTIR spectra provided evidence for the covalent functionalization on the SWCNT (Fig. S7, ESI†). The FTIR spectra of *f*-SWCNTs **1** and **2** are almost featureless, with weak skeletal vibrations of the aromatic domains in the range 1400–1600 $cm.^{-1}$ In the spectra of hybrids **3** and **4**, the C–H stretching vibrations due to the dodecyl chains of the pyrrolidine unit were identified at around 2800–2900 cm^{-1}; the appearance of strong peaks at around ~1450 and ~1600 cm^{-1} (attributed to the C–N bond of the pyrrolidine moiety and to the C=C aromatic stretching) provided significant support for the covalent attachment of pyrrolidine derivative **7** onto the surface of the SWCNTs.

AFM was also employed to study the morphology of the hybrids (Fig. 3). Dilute solutions of *pristine* SWCNT and functionalized samples **3** and **4** in H_2O/SBDS were drop-cast onto SiO_2 surfaces. The resulting images suggest that the SWCNTs have an average height of 1.2 nm (see Fig. S8†). After functionalization the height increased by approximately 2 nm for *f*-SWCNT **3** and 2.5 nm for *f*-SWCNT **4** (Fig. 3). These heights are consistent with the distances calculated for the skeleton structure of the organic addends by means of theoretical calculations using the semiempirical PM3 method implemented on HyperChem 8.0 program package (see Fig. S9†), meaning that the observed increase fits quite well with those expected for these hybrids. TEM was also performed in order to obtain detailed views of the morphology (Fig. S10†). TEM observations

showed that the carbon nanotubes retained the tube-like structure after chemical functionalization, albeit with some defects. Spherical objects were found on the tube walls and these can be attributed to the C_{60} cages (Fig. S10B†).

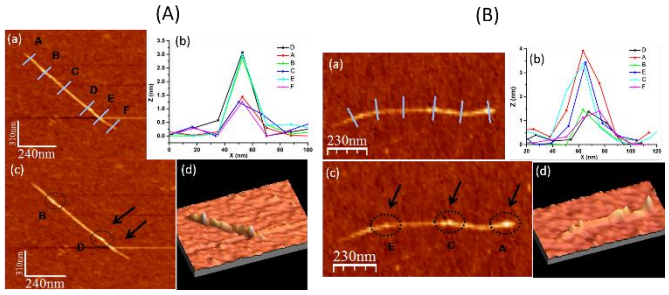

Fig. 3 (a) Topography AFM images of *f*-SWCNT **3** (panel A) and *f*-SWCNT **4** (panel B) on a SiO_2 surface; the Z-profiles indicated with lines A–F are shown in graph (b); (c) AFM images highlighting the functionalized zones; (d) 3-dimensional images of hybrids **3** and **4**.

The electrochemical properties of both hybrids were investigated by Osteryoung square wave voltammetry (OSWV) and the results were compared with those of the reference control derivative **8** (Fig. 4). These studies were performed at room temperature in *o*-dichlorobenzene/acetonitrile (4:1 v/v) containing 0.1 M tetra-*n*-butylammonium hexafluorophosphate ($TBAPF_6$) as supporting electrolyte.

For the control sample **8**, the first cathodic reduction peak was around –1.13 V, which is cathodically shifted compared to the corresponding peak for the parent C_{60} (–1.02 V); this was expected as the saturation of a double bond in the fullerene cage causes a partial loss of conjugation.[50] The characteristic reduction peaks of C_{60} were also observed at –1.19, –1.54 and –2.09 V for the modified *f*-SWCNT **3** and at –1.15, –1.51 and –2.04 V for *f*-SWCNT **4** (see Table S2†). In addition, comparison of the redox potential of the control sample with those of the final hybrids showed cathodic shifts of 60 mV and 20 mV for hybrids **3** and **4**, respectively. The observed shift was attributed to the existence of electronic interactions between the SWCNTs and the fullerene cage. It is important to note that a smaller cathodic shift was expected for *f*-SWCNT **4** when compared to *f*-SWCNT **3** due to the large separation in the former between the C_{60} cage and the nanotube (see Fig. S11†), which decreases the interactions between the two units.

The absorption spectra of suspensions of nanoensembles **3** and **4** in DMF are shown in Fig. S12† along with those of the fullerene control compound **8** and pristine SWCNT. In agreement with literature results, pristine HIPCo showed absorption bands that covered the UV-visible-near infrared regions, thus indicating the presence of SWCNTs of different chirality.[51,52] The strong UV band of SWCNTs was observed at around 250 nm. The control fulleropyrrolidine **8** showed strong absorption bands at 258 and 311 nm along with a sharp peak at 432 nm, which is characteristic of fulleropyrrolidine.[50] In the cases of *f*-SWCNT **3** and *f*-SWCNT **4**, the strong UV band was observed at 275 and 265 nm, respectively, while the visible bands were broadened considerably as a consequence of functionalization of the CNTs and the electronic interactions between the entities – a finding that is consistent with the electrochemical results discussed earlier.

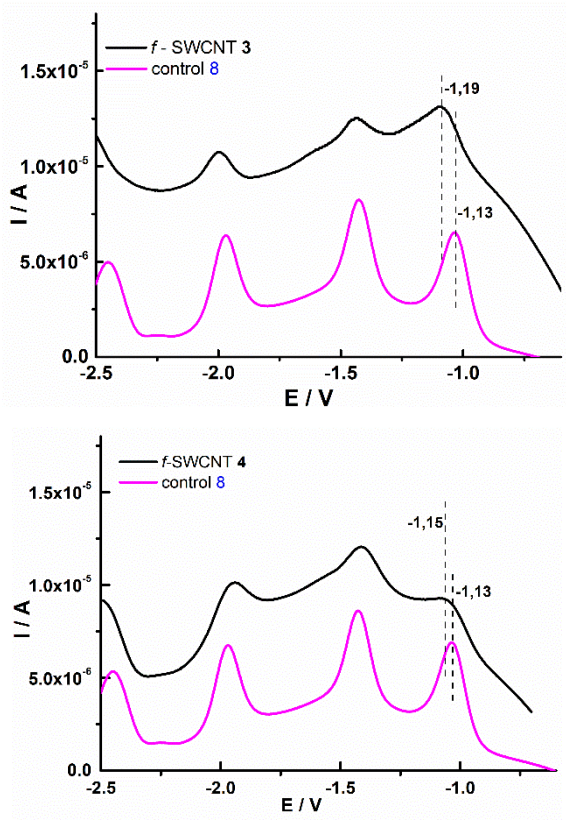

Fig. 4 OSWV (reduction run) of hybrid **3** (top) and hybrid **4** (bottom) compared to that of the control fulleropyrrolidine sample **8**.

It is well known that HIPCo nanotubes dispersed in Sodium Dodecyl Benzene Sulphonate (SDBS) micellar media exfoliate and display photoluminescence spectra that are characteristic of individual semiconducting nanotubes.[53] Experiments performed using the current batch of HIPCo also revealed such luminescence features (data not shown). *f*-SWCNT **3** and *f*-SWCNT **4** were also dispersed in SDBS and their photoluminescence was investigated. However, appreciable luminescence was not observed in these chemically functionalized SWCNTs bearing fulleropyrrolidine moieties. Furthermore, fluorescence of fulleropyrrolidine at 720 nm in the case of *f*-SWCNT **3** and *f*-SWCNT **4** was not observed in NMP, DMF or *o*-DCB, a finding that suggests the occurrence of excited state events in these hybrids.

In order to understand the mechanistic details of the excited state quenching in nanoensembles **3** and **4**, it was important to understand the energetics of photoinduced electron transfer process. Tanaka *et al.*[54] reported the redox potentials of size-sorted SWCNTs by *in situ* photoluminescence spectroelectrochemistry. The oxidation potentials for semiconducting nanotubes found typically in HIPCo ranged between -4.85 to -5.08 V *vs*. vacuum while the reduction potentials ranged between -3.95 to -4.10 V vs. vacuum. The highest HOMO-LUMO gap of 1.08 V was found for SWCNT (8,3) and the lowest was 0.75 V for SWCNT (9,7); these values reveal

diameter/chirality-dependent redox behaviour. The reduction potential of fulleropyrrolidine in the hybrids was -4.2 V *vs.* vacuum (converted from data given in Fig. 4). This suggests promoting an electron to the LUMO level of fullerene from the exciton generated upon photoexcitation of SWCNT is thermodynamically feasible by about 100-150 mV depending upon the chirality of the nanotubes.

In an effort to spectrally characterize the oxidized and reduced SWCNTs, Ehli *et al.*[55] reported on spectroelectrochemical studies where a blue-shift upon reduction and red-shift upon oxidation (p- and n-doping) of SWCNT was observed. It may also be noted that a change in local dielectric constant caused by interactions of solvents and polymers with SWCNTs is known to result in such spectral shifts.[56-57] In the present study, in a complementary experiment, SWCNTs were chemically oxidized using nitrosonium tetrafluoroborate as an oxidizing agent. As shown in Fig. S13, a red-shift about 15 nm of the near-IR peaks were observed. One-electron reduced product of fulleropyrrolidine is known to exhibit a peak in the near-IR region (1000 nm) in the region where strong excitonic peaks of SWCNTs are expected to occur during transient spectral measurements. Importantly, appearance of such signature peaks during transient spectral measurements would provide evidence of electron transfer in the SWCNT-C_{60} nanohybrids.

Next, femtosecond transient absorption studies in two solvents, viz., DMF and NMP were recorded wherein appreciable solubility of the nanohybrids was observed. The samples were excited using 400 and 800 nm laser pulses (100 fs) with pulse energy of about 3 mW. Fig. 5a shows the differential absorption spectra at the indicated delay times of pristine SWCNT and *f*-SWCNT **3** in DMF. The spectra recorded at 1 ps delay time revealed excitonic depleted peaks at 1192, 1335 and 1465 nm. Recovery of these peaks lasted for few tens of ps (see Fig. 5c blue trace for time profile).[55] Interestingly, as shown in Fig. 5b, the transient peaks observed for *f*-SWCNT **3** donor-acceptor hybrid were found to be red-shifted and appeared at 1210, 1353 and 1477 nm. Due to the strong excitonic presence in the 1000 nm range, the relatively weak $C_{60}^{\bullet-}$ peak was difficult to isolate. The time profile of the peak monitored at 1353 nm revealed recovery faster than that observed for pristine SWCNT (see red trace in Fig. 5c) suggesting additional deactivation process, that is, electron transfer from the *in-situ* formed SWCNT exciton to fullerene LUMO level. The recovery process was almost fully completed by 5 ps. These spectral observations were supportive of charge separation from SWCNT exciton to fullerene. Similar observations were also made for *f*-SWCNT **4** donor-acceptor hybrid, however, the red-shift was much smaller (< 10 nm) and the recovery was slower than that observed for *f*-SWCNT **3** (see Fig. 5d for time profile). These suggest relatively slower charge separation in *f*-SWCNT **4** due to increased donor-acceptor distance (see Fig. S11 for donor-acceptor distances).

Similar trends were also seen for donor-acceptor nanohybrids in NMP solvent, as shown in Fig. S14 for *f*-SWCNT **3**. That is, red-shifted excitonic peaks accompanied by faster recovery of these peaks compared to that of pristine SWCNT was observed, supporting occurrence of charge separation. Please note that the spectra were relatively broad in NMP which could be due to the presence of aggregated species in solution.

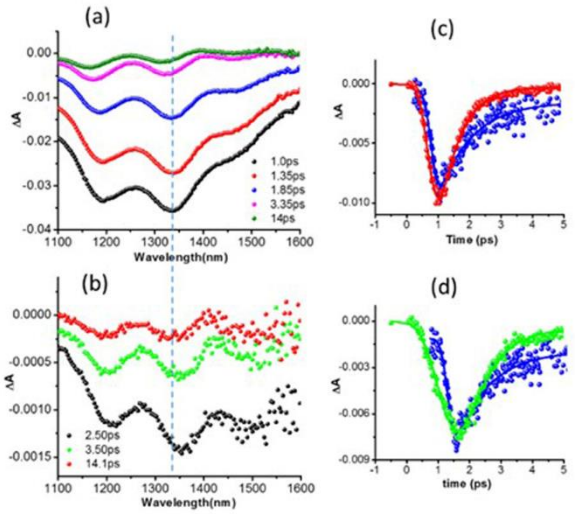

Fig. 5 Femtosecond transient absorption spectra of (a) pristine SWCNT (HIPCo) and (b) *f*-SWCNT **3** in DMF at the excitation wavelength of 400 nm (100 fs pulse width) at the indicated delay times. (c) Time profile of the 1335 nm peak of pristine SWCNT (blue) and 1353 nm peak of *f*-SWCNT **3** (red). (d) Time profile of the 1335 nm peak of pristine SCWNT (blue) and 1327 nm peak of *f*-SWCNT **4** (green).

Next, the nanohybrids were also excited at 800 nm where only the nanotubes and not the fullerene or spacer entity is exclusively excited. As shown in Fig. 6a, excitonic peaks of pristine SWCNTs at 1193, 1332 and 1460 nm that recovered slowly was observed (see Fig. 6c blue trace for time profile). In this case also, the *f*-SWCNT **3** nanohybrid revealed red-shifted peaks at 1225, 1400 and 1485 nm (see spectrum at 1.58 ps delay time in Fig. 6b). The recovering of these peaks was much faster than the pristine SWCNT due to competitive electron transfer in addition to exciton annihilation process. These results support photoinduced charge separation in the newly synthesized SWCNT-fullerene donor-acceptor hybrids.

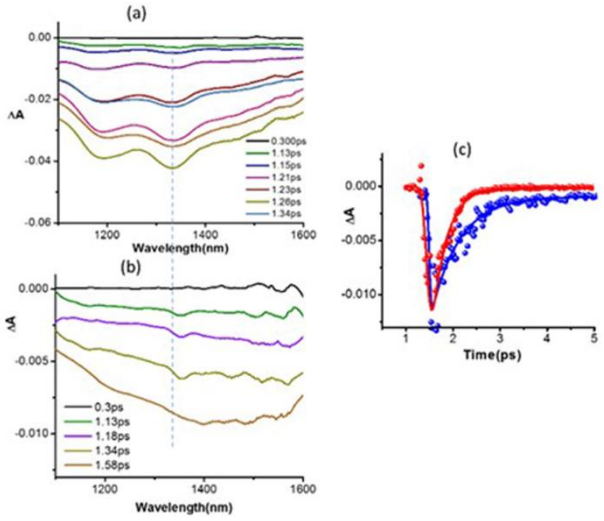

Fig. 6 Femtosecond transient absorption spectra of (a) pristine SWCNT (HIPCo) and (b) *f*-SWCNT **3** in NMP at the excitation wavelength of 800 nm at the indicated delay times.

(c) Time profile of the 1332 nm peak of pristine SWCNT (blue) and 1400 nm peak of *f*-SWCNT **3** (red).

From the time profiles shown in Figs. 5, 6 and S14, time constants for electron transfer obtained were found to be in the range of 3-5 ps resulting in k_{ET} of 2.0 to 3.3 x 10^{11} s^{-1} depending upon the type of hybrid and solvent system. These results reveal ultrafast electron transfer in the SWCNT-fullerene donor-acceptor nanohybrids in which the phenylene-ethynylene spacer groups seem to promote such electron transfer process.

An attempt was also made to evaluate the charge recombination dynamics. For this, femtosecond transient spectra at higher delay times, that is, time period after relaxation of the excitonic peaks, were monitored as shown in Fig. S15. The spectra recorded for pristine SWCNT, at the excitation wavelength of either 400 or 800 nm, revealed weak transient peaks (> 1100 nm) at higher delay times (> 100 ps) that could be attributed to their excited triplet states (Figs. S15a and c).[58] For *f*-SWCNT **3** and **4** hybrids, the transient spectrum recorded at 100 ps (both at 400 and 800 nm excitation) revealed very weak absorbance in the 1000 nm range where $C_{60}^{\bullet-}$ absorbance is expected (Figs. S15b, d and e). Increasing concentration of the sample produced suspensions without improving the signal strength. Intensity of this peak reached almost zero by 3 ns suggesting the time constant for charge recombination is less than 3 ns. Please note that an accurate estimation of charge recombination kinetics was not possible due to very weak signal intensity and the associated uncertainties. From these observations, it is safer to say that the charge separated states persist about 1-2 ns in these donor-acceptor hybrids.

Conclusions

In summary, ultrafast charge separation in oligo(phenylene-ethynylene)-linked SWCNT-C_{60} nanoensembles is demonstrated. The two newly synthesized nanoensembles were fully characterized by a variety of physico-chemical techniques, including TGA, FT-IR, XPS, Raman, AFM, optical absorbance and electrochemical methods. The number of fullerene addends, as estimated by TGA, revealed a moderate level of functionalization without severely jeopardizing the electronic structure of the nanotubes, an observation that was further supported by Raman and FT-IR spectroscopies. Electrochemical studies revealed occurrence of redox processes involving fullerene entities. Evidence for donor (SWCNT)-acceptor (C_{60}) distance (guided by the number of phenylene ethynylene spacer units) dependent electron transfer upon excitation of SWCNT was established from femtosecond transient absorption spectroscopic studies. The present study highlights the importance of all-carbon based donor-acceptor nanoensembles in relevant light harvesting applications.

Acknowledgements

This research was financially supported by the Spanish Ministry of Economy and Competitiveness of Spain (CTQ2013-48252-P and CTQ2015-71936-REDT), Junta de Comunidades de Castilla-La Mancha (PEII-2014-014-P) and the US-National Science Foundation (Grant No. 1401188 to FD). M.B. thanks the MINECO for a doctoral FPI grant.

Notes and references

1 F. D'Souza and O. Ito, *Chem. Soc. Rev*., 2012, **41**, 86–96.
2 M. Vizuete, M. Barrejón, M. J. Gómez-Escalonilla and F. Langa, *Nanoscale*, 2012, **4**, 4370-4381.
3 D. M. Guldi, G. M. A. Rahman, F. Zerbetto and M. Prato, *Acc. Chem. Res.*, 2005, **38**, 871-878.
4 D. M. Guldi and V. Sgobba, *Chem.Commun*., 2011, **47**, 606-610.
5 P. Singh, S. Campidelli, S. Giordani, D. Bonifazi, A. Bianco and M. Prato, *Chem. Soc. Rev.*, 2009, **38**, 2214–2230.
6 N. Martín, L. Sánchez, M. A. Herranz, B. Illescas and D. M. Guldi, *Acc. Chem. Res*., 2007, **40**, 1015-1024.
7 G. Bottari, G. de la Torre, D. M. Guldi and T. Torres, *Chem. Rev*., 2010, **110**, 6768-6816.
8 F. D'Souza and O. Ito, *In Multiporphyrin Array: Fundamentals and Applications*, (Ed. D. Kim), Pan Stanford Publishing: Singapore, 2012, Chapter 8, pp 389-437.
9 F. D'Souza, A. S. D. Sandanayaka and O. Ito, *J. Phys. Chem. Lett*., 2010, **1**, 2586-2593.
10 S. Fukuzumi and K. Ohkubo, *J. Mater. Chem.*, 2012, **22**, 4575-4587.
11 M. S. Arnold, J. L. Blackburn, J. J. Crochet, S. K. Doorn, J. G. Duque, A. Mohite and H. Telg, *Phys. Chem. Chem. Phys*, 2013, **15**, 14896–14918.
12 *Energy Harvesting Materials* (Ed.: D. L. Andrews), World Scientific, Singapore, 2005.
13 S. Gunes, H. Neugebauer and N. S. Sariciftci, *Chem. Rev.*, 2007, **107**, 1324-1338.
14 H. Imahori, T. Umeyama and S. Ito, *Acc. Chem. Res.*, 2009, **42**, 1809-181.
15 T. Umeyama and H. Imahori, *Energy Environ. Sci*., 2008, **1**, 120-133.
16 T. Hasobe, *Phys. Chem. Chem. Phys.*, 2010, **12**, 44-57.
17 P. V. Kamat, *J. Phys. Chem. C*, 2007, **111**, 2834-2860.
18 E. M. Pérez and N. Martín, *Chem. Soc. Rev*., 2008, **37**, 1512-1519.
19 J. N. Clifford, G. Accorsi, F. Cardinali, J. F. Nierengarten and N. Armaroli, *C. R. Chemie.*, 2006, **9**, 1005-1013.
20 V. Balzani, A, Credi and M. Venturi, *ChemSusChem*, 2008, **1**, 26-58.
21 N. Armaroli and V. Balzani, *Angew. Chem. Int. Ed.*, 2006, **46**, 52-66.
22 D. J. Bindl, N. S. Safron, M. S. Arnold, ACS Nano, 2010, 4, 5657-5664.
23 M. P. Ramuz, M. Vosgueritchian, P. Wei, C. Wang, Y. Gao, Y. Wu, Y. Chen and Z. Bao, *ACS Nano*, 2012, **6**, 10384–10395.
24 D. J. Bindl, M.-Y. Wu, F. C. Prehn and M. S. Arnold, *Nano Lett.*, 2010, **11**, 455–460.
25 D. J. Bind and M. S. Arnold, *J. Phys. Chem. C*, 2013, **117**, 2390-2395.
26 R. M. Jain, R. Howden, K. Tvrdy, S. Shimizu, A. J. Hilmer, T. P. McNicholas, K. K. Gleason and M. S. Strano, *Adv. Mater.*, 2012, **24**, 4436–4439.
27 M. J. Shea and M. S. Arnold, *Appl. Phys. Lett.*, 2013, **102**, 243101.
28 Y.Ye, D. J. Bindl, R. M. Jacobberger, M.-Y. Wu, S. S. Roy and M. S. Arnold, *Small*, 2014, **10**, 3299–3306.
29 A. M. Dowgialli, K. S. Mistry, J. C. Johnson and J. L. Blackburn, *ACS Nano*, 2014, **8**, 8573-8581.
30 Q. Zhong, V. diev, S. Roberts, P. Antunez, R. Brutchey, S. Bradforth, M. Thompson, *ACS Nano*, 2013, **7**, 3466-3475.

31 J.-H. Olivier, J. Park, P. Deria, J. Rawson, Y. Bai, A. Kumbhar, M. Therien, *Agew. Chem. Int. Ed*., 2015, **54**, 8133-8138.
32 D. M. Guldi, E. Menna, M. Maggini, M. Marcaccio, D. Paolucci, F. Paolucci, S. Campidelli, M. Prato, G. M. A. Rahman and S. Schergna, *Chem. Eur. J.*, 2006, **12**, 3975-3983.
33 F. D'Souza, R. Chitta, A. S. D. Sandanayaka, N. K. Subbaiyan, L. D'Souza, Y. Araki and O. Ito, *J. Am. Chem. Soc*., 2007, **129**, 15865-15871.
34 F. Ajamaa, T. M. Figueira Duarte, C. Bourgogne, M. Holler, P. W. Fowler, J.-F. Nierengarten, *Eur. J. Org. Chem*., 2005, 3766–3774.
35 J.-J. Hwang and J. M. Tour, *Tetrahedron*, 2002, **58**, 10387–10405.
36 S. Campidelli, B. Ballesteros, A. Filoramo, D. D. Díaz, G. de la Torre, T. Torres, G. M. Aminur Rahman, C. Ehli, D. Kiessling, F. Werner, V. Sgobba, D. M. Guldi, C. Cioffi, M. Prato and J.-P. Bourgoin, *J. Am. Chem. Soc.*, 2008, **130**, 11503–11509.
37 A. Gouloumis, F. Oswald, M. E. El-Khouly, F. Langa, Y. Araki and O. Ito, *Eur. J. Org. Chem.,* 2006, 2344–2351.
38 F. Langa, P. de la Cruz, E. Espíldora, J.J. García, M.C. Pérez-Rodriguez and A. de la Hoz, *Carbon*, 2000, **38**, 1641-1646.
39 M. Barrejón, M. Vizuete, M. J. Gómez-Escalonilla, J. L. G. Fierro, I. Berlanga, F. Zamora, G. Abellán, P. Atienzar, J.-F. Nierengarten, H. García and F. Langa, *Chem. Commun*, 2014, **50**, 9053-9055.
40 M. Vizuete, M. J. Gómez-Escalonilla, J. L. G. Fierro, M, Yudasaka, S. Iijima, M. Vartanian, J. Iehl, J-F Nierengarten and F. Langa, *Chem. Commun*., 2011, **47**, 12771-12773.
41 H.P. Boehm, *Carbon*, 2002, **40**, 145-149.
42 A. Criado, M. Vizuete, M. J. Gómez-Escalonilla, S. García-Rodríguez, J. L. G. Fierro, A. Cobas, D. Peña, E. Guitián and F. Langa, *Carbon*, 2013, **63**, 140-148.
43 M. Barrejón, S. Pla, I. Berlanga, M. J. Gómez-Escalonilla, L. Martín-Gomis, J. L. G. Fierro, M. Zhang, M. Yudasaka, S. Iijima, H. B. Gobeze, F. D'Souza, Á. Sastre-Santos, and F. Langa, *J. Mater. Chem. C*, 2015, **3**, 4960–4969.
44 L. M. Arellano, L. Martín-Gomis, H. B.Gobeze, M. Barrejón, D. Molina, M. J. Gómez-Escalonilla, J. L. G. Fierro, Mi. Zhang, M. Yudasaka, S.Iijima, F. D'Souza, F. Langa and Á. Sastre-Santos, *J. Mater. Chem. C*, 2015, **3**, 10215–10224.
45 A. Jung, R. Graupner, L. Ley and A. Hirsch, *Phys. Stat. Sol*., 2006, **243**, 3217–3220.
46 M. C. Capel, L. Barrio, J. M. Campos-Martín and J. L. G. Fierro, *J. Colloid Interface Sci.* 2004, **277**, 146-153.
47 S. Giordani, J-F Colomer, F. Cattaruzza, J. Alfonsi, M. Meneghetti, M. Prato and Bonifazi, *Carbon*, 2009, **47**, 578 – 588.
48 A. M. M. Omer, S. Adhikari, S. Adhikary, M. Rusop, H. Uchida, M. Umeno and T. Soga, *Physica B*, 2006, **316**, 376-377.
49 A. Criado, M. J. Gómez-Escalonilla, J. L. G. Fierro, A. Urbina, D. Peña, E. Guitián and F. Langa, *Chem. Commun*, 2010, **46**, 7028–7030.
50 M. Maggini, A. Karlson, G. Scorrano, G. Sandona, G. Farnia and M. Prato, *J. Chem. Soc. Chem. Commun.,* 1994, 589-590.
51 R. Chitta, A. S. D. Sandanayaka, A. L. Schumacher, L. D'Souza, Y. Araki, O. Ito and F. D'Souza, *J. Phys. Chem. C*, 2007, **111**, 6947-6955.
52 A. S. D. Sandanayaka,| R. Chitta, N. K. Subbaiyan, L. D'Souza, O. Ito and F. D'Souza, *J. Phys. Chem. C*, 2009, **113**, 13425–13432.
53 M. J. O'Connell, S. M Bachilo, C. B. Huffman, V. C. Moore, M. S. Strano, E. H. Haroz, K. L. Rialon, P. J. Boul, W. H. Noon, C. Kittrell, J. Ma, R. H. Hauge, R. B. Weisman and R. E. Smalley, *Science*, 2002, **297**, 593-596.
54 Y. Tanaka, Y. Hirana, Y. Niidome, K. Kato, S. Saito and N. Nakashima, *Angew*. Chem., Int. Ed., 2009, **48**, 7655–7659.
55 C. Ehli, C. Oelsner, D. M. Guldi, A. Mateo-Alonso, M. Prato, C. Schmidt, C. Backers, F. Hauke and A. Hirsch, *Nature Chem*. 2009, **1**, 243-249.
56 B. A. Larsen, P. Deria, J. M. Holt, I. N. Stanton, M. J. Heben, J. J. Therien, J. L. Blackburn, *J. Am. Chem. Soc*. 2012, **134**, 12485-12491.
57 Y. Maedi, A. Sabara, M. Hashimoto, Y. Hirashima, K. Sode, T. Hasegawa, M. Kanda, M. O. Ishitsuka, T. Tsuchiya, T. Akasaka, T. Okazaki, H. Kataura, J. Lu, S. Nagase, S. Takeuchi, *ChemPhysChem*, 2009, **10**, 926-903.
58 J. Park, P. Deria, M. J. Therien, *J. Am. Chem. Soc*. 2011, **133**, 17156-17159.